The Diurnal Cycle of Precipitation in Tropical Cyclones

KENNETH P. BOWMAN AND MEGAN D. FOWLER

Department of Atmospheric Sciences, Texas A&M University, College Station, Texas

(Manuscript received 26 November 2014, in final form 16 March 2015)

ABSTRACT

Position and intensity data from the International Best Track Archive for Climate Stewardship (IBTrACS) are combined with global, gridded precipitation estimates from the Tropical Rainfall Measuring Mission (TRMM) Multisatellite Precipitation Analysis (TMPA) for the period 1998–2013 to study the diurnal cycle of precipitation in tropical cyclones. The comprehensive global coverage and large sample size afforded by the two datasets allow robust statistical analysis of storm-averaged diurnal variations and permit stratification of the data in various ways. There is a clearly detectable diurnal variation of precipitation in tropical cyclones with peak rainfall occurring near 0600 local time. For storms of all intensities the amplitude of the diurnal harmonic, which dominates the diurnal cycle, is approximately 7% of the mean rain rate. This corresponds to a peak-to-peak variation of about 15% over the course of the day. The diurnal cycle is similar in all ocean basins. There is evidence that the amplitude of the diurnal cycle increases with increasing storm intensity, but the results are not statistically significant. The results have implications for hurricane forecasting and for a greater understanding of the processes that regulate oceanic convection.

1. Introduction

Tropical cyclones pose a significant risk to health and safety for large numbers of people around the globe. Accurate forecasts of hurricane position and intensity are critical for issuing timely storm warnings and evacuation advisories. Hurricane track forecasting has improved substantially in recent years, but improvements in intensity forecasts have come more slowly (Gall et al. 2013). Continuing increases in forecast model resolution and in the representation of physical processes within models will undoubtedly lead to further improvements in forecast skill, but better understanding of the underlying physical processes in tropical cyclones will help to focus research and development efforts in the most promising areas.

One potentially important and predictable component of precipitation variability in tropical cyclones is the diurnal cycle. Precipitation over the oceans in general is known to have a climatological diurnal cycle with maximum rain rates occurring in the early morning hours (Kraus 1963; Gray and Jacobson 1977; Serra and McPhaden 2004; Collier and Bowman 2004; Bowman et al. 2005), although some results are at variance with this. Nesbitt and Zipser (2003) sorted precipitation features by size and intensity using data from the Tropical Rainfall Measuring Mission (TRMM) satellite and found diurnal signals in many characteristics, including an early morning peak in the rain rate. In their analysis of extreme convective events over the ocean near the Indian subcontinent, Romatschke et al. (2010) found that wide convective cores and broad stratiform regions have a broad peak beginning in early to late morning hours, respectively, and extending into the early afternoon. Chen and Houze (1997) found that during the suppressed phase of the Madden–Julian oscillation (MJO), the coldest cloud tops occur near local noon. Combining active and suppressed periods, however, the rainfall peaks in the early morning hours.

A number of studies have examined specifically the diurnal cycle for tropical cyclones. Early observational analyses relied on surface-based observations of diurnal variations in cloudiness or precipitation. Brier and Simpson (1969) found that maximum rain rates in tropical cyclones occur around sunrise and sunset, with minima near noon and midnight. Gray and Jacobson (1977) and Lajoie and Butterworth (1984) also found precipitation

Corresponding author address: Kenneth P. Bowman, Dept. of Atmospheric Sciences, Texas A&M University, 3150 TAMU, College Station, TX 77843-3150.
E-mail: k-bowman@tamu.edu

DOI: 10.1175/JCLI-D-14-00804.1

maxima in the early morning. Using data from small islands in the western Pacific Ocean, Frank (1977) found a diurnal cycle with a peak in the early morning hours and a second larger peak near noon local time. Molinari and Skubis (1985) observed diurnal variations of dynamical variables, including surface pressure and the tangential component of the wind in a case study of Hurricane Agnes. Using five years of sun-synchronous observations from the Special Sensor Microwave Imagers (SSM/I), Rodgers and Pierce (1995) found a diurnal variation in western North Pacific tropical cyclones with a morning maximum and evening minimum. Jiang et al. (2011) used TRMM data to analyze the diurnal cycle of rain in tropical cyclones and found an early morning maximum with an amplitude of about 7%. Dunion et al. (2014) recently demonstrated the existence of a diurnal pulse of cold cloud tops in tropical cyclones that propagates radially outward, but the physical mechanism responsible for the pulse is not clear.

There is some disagreement among the results of these observational studies, which may be as a result of the relatively small number of storms in the observation databases. Some have found a single diurnal peak, while others have reported two peaks, suggesting that there is a significant semidiurnal component to the variability. The timing of the peak rainfall is also not consistent between the different studies. For example, Browner et al. (1977) found a maximum in cloud area at 1700 LST, although the diurnal cycle of cirrus coverage may not necessarily be in phase with diurnal variations of precipitation. The indication, however, is that there is a diurnal cycle of precipitation in tropical cyclones with a maximum in the early morning hours and a minimum in the evening.

Surface-based studies of tropical cyclone precipitation pose a number of problems in addition to the small sample sizes, including the fact that most tropical cyclones form and spend most of their life cycles long distances from sizable landmasses. Surface observations of tropical cyclones at sea are relatively rare, and major changes in hurricane structure take place as the storms make landfall. A modeling study by Tuleya (1994) confirms the potential impact that land surfaces can have on tropical cyclone precipitation cycles. In the model, precipitation associated with a tropical cyclone exhibits a maximum in the late evening and early morning hours when over the ocean, while over land the maximum occurs in the late afternoon.

More recent studies have used satellite data to analyze the diurnal cycle of precipitation in tropical cyclones. Satellites have the significant advantage of providing measurements over large areas of open ocean where surface observations are rare or unavailable. Jiang et al. (2011), for example, used TRMM precipitation data and found a maximum in precipitation between 0430 and 0730 local time, and Wu et al. (2015) found a morning rainfall peak in their study of the radial variation of the diurnal harmonic in tropical cyclones.

Two explanations are commonly offered for the presence of diurnal variation of the intensity of tropical cyclones. The first is related to the S_2 atmospheric tide, which has been used to explain the presence of a semidiurnal cycle in tropical cyclones (Brier and Simpson 1969; Kossin 2002). A diurnal signal with a single peak has been hypothesized to result from differential heating between cloudy and clear areas or diurnal variations in radiational heating of the cloud tops by solar radiation (Gray and Jacobson 1977; Hobgood 1986; Randall et al. 1991).

The goal of this study is to determine whether a diurnal cycle of precipitation rates exists in tropical cyclones and to establish statistical estimates of its magnitude and timing. In this study we combine a 15-yr record of 3-hourly satellite precipitation estimates with tropical cyclone track data to estimate the amplitude and phase of the climatological diurnal and semidiurnal harmonics of precipitation in tropical cyclones. The large sample size provided by the global satellite coverage allows us to make firm error estimates, to stratify the data by storm intensity and by ocean basin, and to evaluate the influence of nearby land surfaces on the diurnal cycle.

2. Data

a. *Hurricane track data*

The International Best Track Archive for Climate Stewardship (IBTrACS) is a global record of tropical cyclone track and intensity information maintained by NOAA's National Climatic Data Center (2014; Knapp et al. 2010). Records are compiled from analyses by a number of meteorological agencies around the world. Storm parameters are typically recorded at 0000, 0600, 1200, and 1800 UTC, although some observations are available at special times because of unique conditions of the storm. In this study we use the 6-hourly observations for the period 1998–2012 from the IBTrACS-All database. The availability of satellites and other modern observing systems throughout the selected period make the track data relatively homogeneous and of good quality.

b. *Precipitation data*

Precipitation estimates corresponding to the storm locations in the IBTrACS dataset are taken from version 7 of the TRMM Multisatellite Precipitation Analysis (TMPA) (Huffman et al. 2007; 2014). This product is also referred to as 3B42 data. TMPA rain-rate data are available for the entire study period from 1998 to 2012.

The TMPA is based primarily on measurements from microwave imaging radiometers on multiple satellites. When observations from imagers are unavailable, the algorithm uses rain estimates from the Advanced Microwave Sounding Unit (AMSU) radiometer. When no microwave data are available, the algorithm uses precipitation estimates from geostationary IR imagers, where available. Cecil and Wingo (2009) and Zagrodnik and Jiang (2013) compared TRMM Microwave Imager (TMI) and Precipitation Radar (PR) rainfall retrievals for tropical cyclones and found that the TMI tends to underestimate rain rates relative to the PR in areas of heavy precipitation, particularly in the inner core and inner rainbands. Liu and Zipser (2014) found similar results of oceanic precipitation in general. The TMPA algorithm use the TRMM TMI–PR combined retrieval (TCI; 2B31 data) for calibration of the microwave retrievals, which may improve the retrievals of heavy rain in tropical cyclones, but a detailed comparison of the TMPA with PR for tropical cyclones has not been carried out.

The TMPA data cover the latitude zone from 50°S to 50°N. Data consist of area-averaged precipitation rates for 0.25° × 0.25° longitude–latitude grid boxes at 3-h intervals centered on the nominal observing times of 0000, 0300, . . . , 2100 UTC. Within each 3-h window, if observations are available for a grid box from multiple microwave instruments, the values are averaged using simple arithmetic averaging. To evaluate the possible influence of land on precipitation within storms, we use the NOAA/National Geophysical Data Center (NGDC) TerrainBase dataset, a global 5′ longitude–latitude land elevation and ocean depth digital terrain model (DTM) database, to calculate the land fraction within each TMPA grid box (NGDC 2004).

3. Methods

a. Hurricane track data

To create the largest possible sample of storms and rain rates, we use data from all ocean basins. Storms occasionally move from one basin to another during their lifetimes, so individual storms are labeled by their genesis basin. See Table 1 for a list of the genesis basins and the percentage of storms that originated in each basin. When the data are stratified by basin, the South Atlantic basin is excluded because it has too few storms in the data record to provide useful statistics. To make better use of the available TMPA data and to provide more information about the diurnal variation of precipitation within storms, the 6-hourly IBTrACS storm positions are interpolated linearly in time to 0300, 0900, 1500, and 2100 UTC, which gives eight daily positions that correspond to the nominal TMPA observing times.

TABLE 1. Observations in the IBTrACS dataset for the study period 1998–2012 by ocean basin ordered by the number of observations in each basin. The basins here (and in Table 4) are ordered by number of observations from largest to fewest.

Ocean basin	Percent of obs	No. of storms
Western Pacific	29.65%	415
Southern Indian	22.12%	255
Eastern Pacific	16.29%	268
North Atlantic	15.86%	241
South Pacific	10.86%	154
Northern Indian	5.08%	127
South Atlantic	0.14%	3

The IBTrACS database includes storm location and intensity observations (wind speed and central pressure) from up to 25 meteorological agencies, and many storms have reports from multiple agencies. For this analysis we use the first available position report in the IBTrACS database according to the priority list in Table 2. Averaging across all basins and storm intensities, the mean angular distance between the average location of a storm and the individual estimates from the input sources is 0.08°, and only 0.25% of storm observations have a distance between the mean location and any individual estimate that is greater than 1°. Because the position differences between the reporting agencies are generally less than the resolution of the TMPA precipitation grid, the scatter in storm positions from the various input sources has little or no effect on the storm-averaged precipitation estimates used to investigate the diurnal cycle.

b. TMPA data

For each 3-hourly storm position, the area-averaged precipitation for the storm is estimated from the TMPA gridded precipitation data by averaging the gridded rain rates over a circle with a radius of 500 km centered on the storm location. This is consistent with other studies (e.g., Rogers and Adler 1981; Lonfat et al. 2004) and should capture the primary circulation for all except the largest storms (Frank 1977). We tested a range of radii for the averaging areas and found similar results. Larger radii tend to include nonraining areas outside the storm, which reduces both the mean rain rate and the amplitude of the diurnal cycle, so the average rain rate will depend on the radius of the averaging area. Wu et al. (2015) have analyzed the radial dependence of the diurnal cycle in tropical cyclones using similar methods.

TABLE 2. Priority order for sources of data in the IBTrACS database and percentage of observations from each data source for this study.

Priority	Source	Percent of obs
1	HURDAT (NOAA Hurricane Database)	30.89%
2	Joint Typhoon Warning Center	54.23%
3	Central Pacific Hurricane Center	0.00%
4	Regional Specialized Meteorological Center, Tokyo	3.83%
5	Shanghai Typhoon Institute	0.72%
6	Hong Kong Observatory	0.05%
7	Tropical Cyclone Warning Center, Darwin	2.46%
8	Tropical Cyclone Warning Center, Wellington	1.39%
9	Regional Specialized Meteorological Center, New Delhi	2.16%
10	Regional Specialized Meteorological Center, La Réunion	3.63%
11	Automated Tropical Cyclone Forecast (U.S. Navy)	0.20%
12	Regional Specialized Meteorological Center, Nadi	0.40%
13	C. Neumann's Southern Hemisphere data	0.04%
14	University Corporation for Atmospheric Research	0.00%
15	National Climatic Data Center	0.00%

To estimate the diurnal variation of precipitation, it is necessary to know the local time at which the observations were made. The TMPA data files include information about the times within each 3-h window that different satellites observed each grid box. Unfortunately, the TMPA grid for a single storm is frequently a complex geographic mosaic of observations from different instruments at different times. See Fig. 1 in Huffman et al. (2007) for an example of the variety of data sources in a single 3-h grid. Also, precipitation estimates from the geostationary IR instruments are all reported at the nominal observing times (0000, 0300 UTC, etc.). For consistency and simplicity we have chosen to compute the local time corresponding to each 3-hourly TMPA observation by using the storm longitude and the nominal synoptic observation time. The local time in hours is related to the UTC time by $t_{\text{local}} = [t_{\text{UTC}} + \lambda(24/360)] \bmod 24$, where λ is the longitude of the storm center (0°–360°). This approximation will introduce small errors in the assignment of the observation time for the precipitation measurements, but these errors should be random with an average of zero and a maximum possible value of 1.5 h.

Because the IR precipitation estimates are based on the presence of cold cloud tops, which is related indirectly to the precipitation rate, we compute the area-averaged rain rates both with and without the IR data in order to evaluate whether the use of IR data has an effect on the timing or amplitude of the observed diurnal cycle. We also stratify the data by land fraction to determine whether interactions with land areas have an influence on the diurnal cycle. Passive microwave precipitation retrievals are more difficult over land than ocean, primarily because of variations in land surface emissivity. Liu and Zipser (2014) compared rain retrievals from the TRMM Microwave Imager with the PR, which is much less sensitive to the properties of the underlying surface. They found complex geographic and precipitation-regime dependencies in the differences between the two instruments, and recommend further ground-truth studies over the ocean, in particular. While it will not necessarily resolve all rain-rate-dependent biases, the TMPA product is both calibrated with the TRMM PR and adjusted to match monthly mean rain gauge data over land.

c. Analysis

We characterize the climatological diurnal cycle of the rain rate R in terms of Fourier harmonics by fitting sines and cosines to $R(t)$ using least squares regression:

$$R_i(t_i) = R_0 + \sum_{k=1}^{N}\left[a_k \cos\left(\frac{2\pi k t_i}{\tau}\right) + b_k \sin\left(\frac{2\pi k t_i}{\tau}\right)\right] + \varepsilon_i, \tag{1}$$

where R_i is the rain rate; t_i is the local time of the observation; $i = 1, \ldots, M$; R_0 is the mean rain rate; k is the harmonic index; N is the maximum harmonic index used in the fit (typically 8); a_k and b_k are the amplitudes of the cosine and sine terms of the kth harmonic, respectively; τ is the length of the day in the same units as t_i; and ε_i is the residual.

Equation (1) can be written as

$$R_i(t_i) = R_0 + \sum_{k=1}^{N} A_k \cos\left(\frac{2\pi k t_i}{\tau} - \phi_k\right) + \varepsilon_i, \tag{2}$$

where the amplitude A_k and phase ϕ_k of harmonic k are

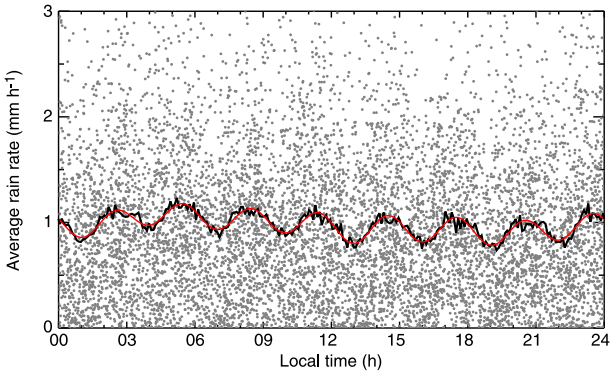

FIG. 1. Area-averaged rain rates for all storm observations as a function of local time (gray dots). Each dot represents the area-averaged rain rate for one storm at one time. For clarity only every tenth point is plotted. Approximately 1.5% of the rain rates are greater than 3 mm h^{-1} and are not plotted. The black line is the rain rates averaged into 256 equal-sized time bins. The red curve is the fit to the binned data using eight harmonics. The obvious harmonic 8 is an artifact of the eight-times-daily sampling of the TMPA data that can be removed to reveal the diurnal and semidiurnal harmonics.

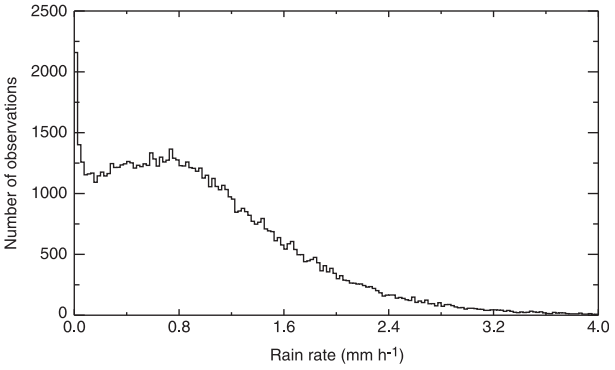

FIG. 2. Histogram of area-averaged rain rates for all observations. The bin size is 0.025 mm h^{-1}. The total number of observations is 85 932 and the mean rain rate is 0.98 mm h^{-1}.

$$A_k = \sqrt{a_k^2 + b_k^2} \tag{3}$$

and

$$\phi_k = \tan^{-1}\left(\frac{b}{a}\right). \tag{4}$$

Assuming that the residuals ε_i follow a Gaussian distribution, confidence limits for the regression coefficients can be estimated from the F distribution with 2 and $M - (N + 1)$ degrees of freedom.

4. Results

a. The diurnal cycle

The data used in this analysis consist of the following parameters for each tropical cyclone observation: the longitude and latitude of the storm center, the local time t, the genesis basin, the maximum sustained wind speed (translated to intensity on the Saffir–Simpson scale), the area-averaged rain rate for a 500-km circle centered on the storm location, and the fraction of each averaging circle f that is land.

Figure 1 shows the area-averaged rain rates for all storms in the data record as a function of local time t. For clarity only 10% of the data points are plotted and the maximum value shown is 3 mm h^{-1}. Approximately 1.5% of the storm-averaged rain rate values are greater than 3 mm h^{-1} and are not displayed. As expected, the likelihood of occurrence of a given rain rate generally decreases as the rain rate increases. Figure 2 is a histogram of rain rates for all storms. Despite the substantial area and time averaging used to compute the rain rate for an individual storm observation, the resulting values are distinctly non-Gaussian. It is possible to estimate the harmonics of the diurnal cycle using the raw data in Fig. 1, but to allow robust statistical estimates of the uncertainties in the amplitudes and phases of the diurnal harmonics, the individual observations are further averaged by binning into M equal-sized bins by local time. The choice of M involves trade-offs between the amount of smoothing and the number of degrees of freedom retained in the time series. We tested the sensitivity of the statistics to the value of M by using M equal to powers of 2 between 8 and 1024. The results are not strongly sensitive to the value of M for $M \geq 64$. Using $M = 256$ gives good estimates of statistical error and provides a large enough sample size to evaluate the Gaussianity of the residuals. The binned values are plotted as the black line in Fig. 1. These binned rain-rate values and the central times of each bin are used as the analysis variables R_i and t_i in Eq. (1). The result of fitting the binned values with eight harmonics ($N = 8$) is plotted as the red curve in Fig. 1. A histogram of the residuals ε_i is plotted in Fig. 3, along with a Gaussian distribution with the same mean and standard deviation as the residuals. As can be seen, the additional averaging into the 256 time bins is sufficient to render the residuals Gaussian to a good approximation.

The binned values in Fig. 1 have a prominent $k = 8$ component that is an artifact resulting from interactions between the eight-times-daily TMPA sampling, the nonuniform longitudinal distribution of the storms, and systematic variations in storm intensity with longitude. Figure 4 is a histogram of the longitudes of the storm centers for all observations. The largest peak in longitudes is in the western Pacific from around 105° to 160°E, which is not surprising given the frequency of storm

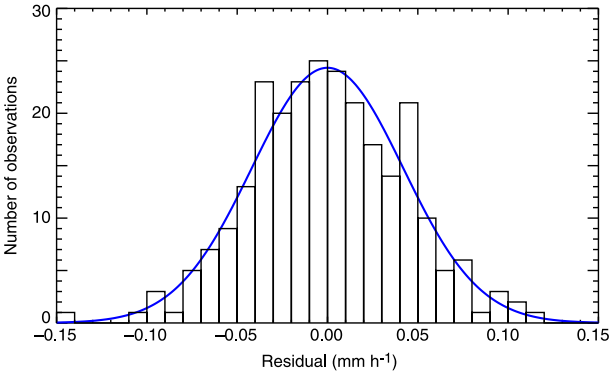

FIG. 3. Histogram of residuals from the regression for rain rates that were averaged into 256 time bins. The blue curve is a Gaussian with the same mean and standard deviation as the data.

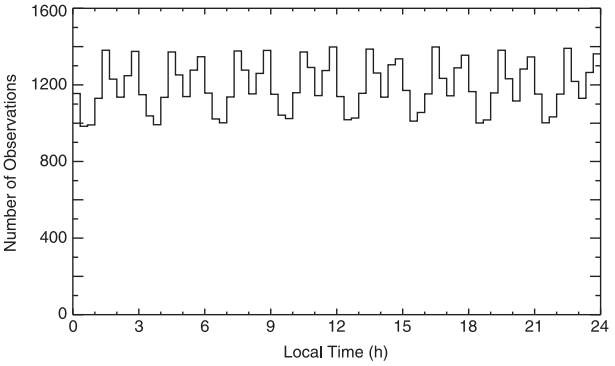

FIG. 5. Histogram of the local observation time for all storm observations.

occurrence by basin in Table 1. The nonuniform distribution of longitudes leads to a nonuniform distribution of local observation times. Figure 5 is a histogram of the local time of the observations; it reveals a distinct 3-hourly signal in the local time of observation. This systematic sampling bias and the correlation between storm longitude and intensity introduces the spurious $k = 8$ component of diurnal variation seen in Fig. 1. The $k = 8$ component could be removed by averaging the data into eight diurnal bins, but that would result in the loss of information that is useful for estimating the errors in the fit parameters a_k and b_k. Therefore, the $k = 8$ component is removed by fitting the data with all harmonics up to $k = 8$ and subtracting the fitted harmonic 8 from the data. The result of this procedure is shown as the black line in Fig. 6, along with the individual diurnal and semidiurnal harmonics ($k = 1$ and 2, respectively). The intermediate harmonics ($k = 3$ through 7) are not shown, as statistically they are not significantly different from zero.

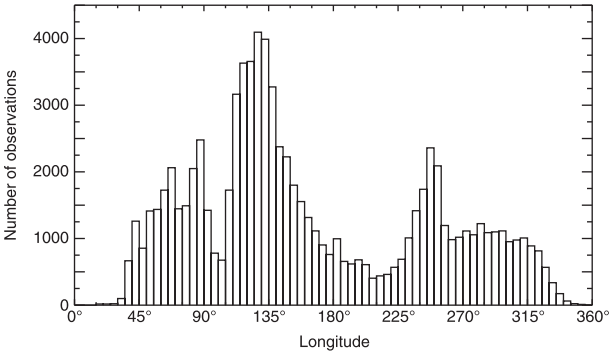

FIG. 4. Histogram of storm center longitudes for all storm observations. The longitudes on the x axis start at the prime meridian and advance eastward.

In the top-right-hand corner of Fig. 6, the amplitude and phase of the globally averaged diurnal (red) and semidiurnal (blue) harmonics are plotted in vector format. The diurnal and semidiurnal harmonics are nearly in phase, with peaks near 0600 local time (LT). Although the semidiurnal harmonic is much smaller than the diurnal harmonic, the effect of the in-phase relationship is to slightly increase the mean rain rate near both the 0600 LT peak and the 1800 LT minimum. This acts to increase the morning peak and flatten the afternoon minimum. The gray circles at the tip of each vector are 95% confidence intervals, estimated as in Anderson (1971). The amplitudes of the two components are small compared to the mean rain rate, which is approximately 1 mm h^{-1}, but both are statistically different from zero.

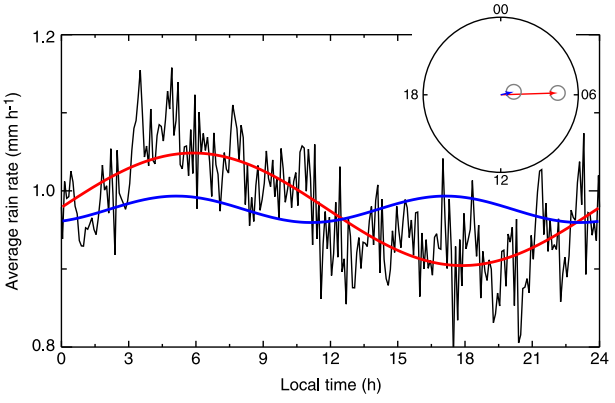

FIG. 6. Binned rain rates for all observations in all basins (black line) with harmonic 8 removed. The diurnal and semidiurnal harmonics from the least squares fit are plotted in red and blue, respectively. In the top-right corner the amplitude and phase (local time of day) of the two harmonics are plotted as vectors using the same colors. The radius of the outer circle corresponds to 0.1 mm h^{-1}. The small gray circles are the 95% confidence limits on the estimates of each harmonic.

TABLE 3. Mean rain rate and amplitude and phase of the diurnal harmonic for all data and with IR data omitted.

Data	R_0 (mm h^{-1})	A_1 (mm h^{-1})	ϕ_1 (h)	No. of samples
All	0.98 ± 0.01	0.07 ± 0.01	5.9 ± 0.5	85 932
No IR	0.94 ± 0.01	0.06 ± 0.01	6.0 ± 0.7	76 619

b. Impact of IR data

The TMPA data use precipitation estimates from geostationary IR imagery when microwave data are not available. To test whether including the IR data has an impact on the regression, the analysis is repeated using only microwave data when computing the storm-averaged rain rates. The results are given in Table 3. Because the observations for some storms contain only IR data, eliminating the IR data reduces the number of observations available by about 11% (column 5). Including the IR data slightly increases the estimate of the mean rain rate (column 2). This difference is statistically significant at better than the 95% level and suggests a small bias between the microwave and IR rain-rate retrievals, at least for tropical cyclones. Kikuchi and Wang (2008) found a 3-h phase difference between the TMPA data with IR included, and the TRMM TMI–PR combined rainfall 3G68 product, which does not use any IR data. Here, however, we find that the differences between the amplitudes and phases of the diurnal harmonic (columns 3 and 4) with and without IR data are not statistically significant. In both cases the amplitude of the diurnal harmonic is about 7% of the mean values, and the peak rainfall occurs near 0600 LT.

c. Stratification by basin

The result of stratifying rain-rate observations by basin is shown in Table 4. These results use all available observations within each basin. Mean rain rates vary substantially among the basins, with a minimum of 0.60 mm h^{-1} in the eastern Pacific and a maximum of 1.24 mm h^{-1} in the western Pacific. In all basins the amplitude of the diurnal harmonic is different from zero at greater than a 95% confidence level, although the error bars are somewhat larger than for the global average because of the smaller sample sizes. The peak rainfall in all basins clusters around 0600 LT, although the peak occurs earlier in the two Southern Hemisphere basins. The reason for this difference is not known.

The data in Table 4 suggest that the amplitude of the diurnal harmonic might depend on the mean rain rate. The values from the table are plotted in Fig. 7, along with a linear fit to the plotted data. The data suggest that higher mean rain rates are associated with larger amplitude diurnal cycles. The correlation in this case is 0.55; but, because of the small number of points, the slope of the regression line (0.04) is not significantly different from zero at the 95% level and no firm conclusion can be made.

d. Stratification by intensity

Results of stratifying the rain-rate observations by storm intensity are given in Table 5. Storm intensity is computed from the maximum sustained wind speed data in the IBTrACS database. Here we follow the U.S. convention of classifying storms identified as category 4 or 5 on the Saffir–Simpson scale as strong hurricanes, while those in categories 1–3 are classified as weak hurricanes. Tropical cyclones that do not reach hurricane strength are classified as tropical storms.

Because the frequency with which storms occur decreases with intensity, the number of observations of strong hurricanes in particular is small. Only 21% of the observations are of hurricanes (strong and weak combined). The majority of observations in the database are of tropical storms (79%). As a result, the global average statistics are dominated by relatively weak storms. The mean rain rate clearly depends on storm intensity. Unsurprisingly, stronger storms have higher average rain rates. The results for the amplitude of diurnal harmonic are not as clear. Strong hurricanes have the largest diurnal variation, followed by tropical storms and then weak hurricanes. In all cases the amplitudes of the diurnal harmonic are statistically different from zero but are not statistically different from each other, so it is not possible to conclude that the amplitude of the diurnal harmonic depends on storm intensity. The timing of the peak rainfall clusters around 0600–0700 local time for all intensity classes.

TABLE 4. Mean rain rate and amplitude and phase of the diurnal harmonic stratified by genesis basin.

Ocean basin	R_0 (mm h^{-1})	A_1 (mm h^{-1})	ϕ_1 (h)	No. of samples
Western Pacific (WP)	1.24 ± 0.01	0.08 ± 0.02	6.8 ± 0.8	25 479
Southern Indian (SI)	0.87 ± 0.01	0.09 ± 0.02	4.1 ± 0.8	19 014
Eastern Pacific (EP)	0.60 ± 0.01	0.06 ± 0.02	6.5 ± 1.2	14 000
North Atlantic (NA)	0.92 ± 0.01	0.06 ± 0.02	7.9 ± 1.4	13 632
South Pacific (SP)	1.09 ± 0.01	0.10 ± 0.03	3.0 ± 1.1	9325
Northern Indian (NI)	1.00 ± 0.02	0.09 ± 0.07	7.5 ± 3.9	4363

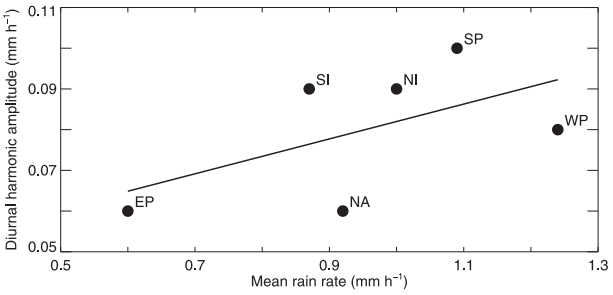

FIG. 7. Amplitude of the diurnal harmonic A_k as a function of mean rate R_0 for the different genesis basins. See Table 4 for the two letter designations of the genesis basins.

e. *Effects of interaction with land*

The character of tropical cyclones changes quickly as they make landfall or pass over mountainous islands. To evaluate whether interaction with land surfaces has an effect on the diurnal cycle of precipitation, the data are stratified into three categories according to the fraction of land f within the 500-km-averaging circle centered on the storm location. The results are given in Table 6. For the first two categories, with $f < 1/3$ and f between $1/3$ and $2/3$, the results are essentially the same, with peak rainfall occurring near 0600 local time. This suggests that either interaction with land surfaces does not have a large effect on the diurnal behavior, even when land occupies a substantial fraction of the storm area, or that the adjustment time to the different surface conditions is comparable to the time it takes for storms to move inland, so storms retain their oceanic character for a time as the land fraction increases. In the IBTrACS database, only about 2% of the storm position reports have $f > 2/3$. Because of the small sample size, the amplitude of the diurnal harmonic for that category is not statistically distinguishable from zero, although the results suggest that there might be a reduction in the amplitude of the diurnal cycle and a shift to a peak rainfall before midnight local time. This result could also be due to situations where the portion of the storm over land has a different diurnal cycle than the portion that remains over the ocean. When averaged together the result is a weak diurnal cycle.

5. Discussion and conclusions

This study combines track data from the International Best Track Archive for Climate Stewardship (IBTrACS) database and eight-times-daily gridded precipitation estimates from the TRMM Multisatellite Precipitation Analysis to investigate the diurnal cycle of precipitation in tropical cyclones. The 15-yr global record of precipitation from the TMPA includes over 85 000 observations of individual tropical cyclones. With the large sample size, a robust statistical analysis of the properties of the climatological diurnal cycle in tropical cyclones is possible.

Precipitation in tropical cyclones has a clearly detectable diurnal cycle with a maximum near 0600 local time. The diurnal variation is dominated by the first diurnal harmonic. A weak semidiurnal component that is in phase with the diurnal harmonic is also present. Higher harmonics are not statistically significant. Averaged over all ocean basins and all storm intensities, the amplitude of the diurnal harmonic in tropical cyclones is approximately 7% of the mean rain rate. This is consistent with recent analyses by Jiang et al. (2011) and Wu et al. (2015), but smaller than the diurnal amplitude for all oceanic precipitation of about 15% in Fig. 7 of Nesbitt and Zipser (2003) and Fig. 10 of Bowman et al. (2005). This suggests that the precipitation rate in tropical cyclones may be determined less by diurnal radiative forcing and more by the dynamical organization of the storm than is the case for tropical oceanic precipitation in general.

Average rainfall rates in tropical cyclones vary by a factor of 2 among the different ocean basins. With the exception of the South Atlantic basin, where the number of storms in the data record is too small to allow statistical analysis, tropical cyclones exhibit a diurnal cycle with a morning maximum in all of the major ocean basins. Based on stratifying the data by basin and by storm intensity, there is evidence that the amplitude of the diurnal cycle increases as the mean rainfall rate increases, but that result is not statistically significant. This would be consistent with the results in Fig. 10 of Bowman et al. (2005), which show that the amplitude of the diurnal cycle over the tropical oceans is proportional to the mean rain rate over a relatively wide range of rain

TABLE 5. Mean rain rate R_0 and the amplitude A_1 and phase ϕ_1 of the diurnal harmonic stratified by storm intensity. Intensity categories are based on the maximum sustained wind speed V_{max} (1 kt $\approx$ 0.51 m s^{-1}).

Intensity	V_{max} (kt)	R_0 (mm h^{-1})	A_1 (mm h^{-1})	ϕ_1 (h)	No. of samples
Strong hurricanes (categories 3–5)	≥96	1.65 ± 0.02	0.10 ± 0.06	7.1 ± 2.2	3158
Weak hurricanes (categories 1 and 2)	64–95	1.30 ± 0.01	0.06 ± 0.03	6.9 ± 1.9	14 527
All hurricanes	≥64	1.37 ± 0.01	0.07 ± 0.03	6.9 ± 1.6	17 685
Tropical storms	<64	0.88 ± 0.01	0.08 ± 0.02	5.8 ± 1.0	68 247

TABLE 6. Mean rain rate and amplitude and phase of the diurnal harmonic stratified by land fraction. For the category with $f > 2/3$, the number of time bins is reduced to 32 to avoid empty bins. Even so, the 95% confidence circle includes the origin, so it is not possible to compute the uncertainty in the phase.

Land fraction f	R_0 (mm h^{-1})	A_1 (mm h^{-1})	ϕ_1 (h)	No. of samples
$0 \le f < 1/3$	0.98 ± 0.02	0.08 ± 0.02	5.8 ± 1.2	71 354
$1/3 \le f < 2/3$	0.97 ± 0.02	0.06 ± 0.03	7.2 ± 2.0	12 694
$2/3 \le f < 1$	0.75 ± 0.05	0.04 ± 0.09	−2.2	1884

rates. The number of identifiable tropical cyclones over land is small in the IBTrACS database, so it is not possible to draw strong conclusions about how interactions with land might modify the diurnal cycle.

The results of this study imply a total variation in precipitation in tropical cyclones of about 15% over the course of the day between the morning maximum and afternoon minimum, although the diurnal range may be even larger in the core of tropical systems (Wu et al. 2015). A variation of this magnitude has implications for forecasting storm intensity at landfall, and it raises interesting questions about the mechanisms responsible for the diurnal cycle of precipitation of the ocean and whether those mechanisms are properly represented in current numerical forecast models.

Acknowledgments. The IBTrACS dataset was obtained from the NOAA/National Climatic Data Center (https://www.ncdc.noaa.gov/ibtracs/index.php). We thank everyone involved for their work to create a high-quality, homogenous tropical cyclone database. The TRMM Multisatellite Precipitation Analysis data were obtained from NASA Goddard Earth Sciences Data and Information Services Center (http://disc.sci.gsfc.nasa.gov/gesNews/trmm_v7_multisat_precip). We thank the TRMM Science and Precipitation Measurement Teams for use of the data, and Dr. Qiaoyan Wu for helpful discussions and comments on the manuscript. We also thank Dr. Ed Zipser and two anonymous reviewers for their valuable comments on the manuscript.

REFERENCES

Anderson, T. W., 1971: *The Statistical Analysis of Time Series.* John Wiley & Sons, 704 pp.

Bowman, K. P., J. C. Collier, G. R. North, Q. Wu, E. Ha, and J. Hardin, 2005: The diurnal cycle of tropical precipitation in TRMM satellite and ocean buoy rain gauge data. *J. Geophys. Res.,* **109,** D06115, doi:10.1029/2005JD005763.

Brier, G. W., and J. Simpson, 1969: Tropical cloudiness and rainfall related to pressure and tidal variations. *Quart. J. Roy. Meteor. Soc.,* **95,** 120–147, doi:10.1002/qj.49709540309.

Browner, S. P., W. L. Woodley, and C. G. Griffith, 1977: Diurnal oscillation of the area of cloudiness associated with tropical storms. *Mon. Wea. Rev.,* **105,** 856–864, doi:10.1175/1520-0493(1977)105<0856:DOOTAO>2.0.CO;2.

Cecil, D. J., and M. Wingo, 2009: Comparison of TRMM rain-rate retrievals in tropical cyclones. *J. Meteor. Soc. Japan,* **87A,** 369–380, doi:10.2151/jmsj.87A.369.

Chen, S. S., and R. A. Houze, 1997: Diurnal variation and life-cycle of deep convective systems of the tropical Pacific warm pool. *Quart. J. Roy. Meteor. Soc.,* **123,** 357–388, doi:10.1002/qj.49712353806.

Collier, J. C., and K. P. Bowman, 2004: Diurnal cycle of tropical precipitation in a general circulation model. *J. Geophys. Res.,* **109,** D17105, doi:10.1029/2004JD004818.

Dunion, J. P., C. D. Thorncroft, and C. S. Velden, 2014: The tropical cyclone diurnal cycle of mature hurricanes. *Mon. Wea. Rev.,* **142,** 3900–3919, doi:10.1175/MWR-D-13-00191.1.

Frank, W. M., 1977: The structure and energetics of the tropical cyclone I. Storm structure. *Mon. Wea. Rev.,* **105,** 1119–1135, doi:10.1175/1520-0493(1977)105<1119:TSAEOT>2.0.CO;2.

Gall, R., F. Toepfer, F. Marks, and E. Rappaport, 2013: Hurricane forecast improvement project years five to ten strategic plan. NOAA Tech. Rep. HFIP2014-1, 44 pp.

Gray, W. M., and R. W. Jacobson, 1977: Diurnal variation of deep cumulus convection. *Mon. Wea. Rev.,* **105,** 1171–1188, doi:10.1175/1520-0493(1977)105<1171:DVODCC>2.0.CO;2.

Hobgood, J. S., 1986: A possible mechanism for the diurnal oscillations of tropical cyclones. *J. Atmos. Sci.,* **43,** 2901–2922, doi:10.1175/1520-0469(1986)043<2901:APMFTD>2.0.CO;2.

Huffman, G. J., R. F. Adler, D. T. Bolvin, G. Gu, E. J. Nelkin, K. P. Bowman, E. F. Stocker, and D. Wolff, 2007: The TRMM Multisatellite Precipitation Analysis (TMPA): Quasi-global, multi-year, combined-sensor precipitation estimates at fine scales. *J. Hydrometeor.,* **8,** 38–55, doi:10.1175/JHM560.1.

——, D. T. Bolvin, E. J. Nelkin, and R. F. Adler, 2014: Version 7 TRMM Multi-satellite Precipitation Analysis (TMPA) 3B42. Goddard Earth Sciences Data and Information Services Center. Subset used: 1998–2012, accessed 25 May 2012. [Available online at http://disc.sci.gsfc.nasa.gov/nrt/gesNews/trmm_v7_multisat_precip.]

Jiang, H., C. Liu, and E. J. Zipser, 2011: A TRMM-based tropical cyclone cloud and precipitation feature database. *J. Appl. Meteor. Climatol.,* **50,** 1255–1274, doi:10.1175/2011JAMC2662.1.

Kikuchi, K., and B. Wang, 2008: Diurnal precipitation regimes in the global tropics. *J. Climate,* **21,** 2680–2696, doi:10.1175/2007JCLI2051.1.

Knapp, K. R., M. C. Kruk, D. H. Levinson, H. J. Diamond, and C. J. Neumann, 2010: The international best track archive for climate stewardship. *Bull. Amer. Meteor. Soc.,* **91,** 363–376, doi:10.1175/2009BAMS2755.1.

Kossin, J. P., 2002: Daily hurricane variability inferred from GOES infrared imagery. *Mon. Wea. Rev.,* **130,** 2260–2270, doi:10.1175/1520-0493(2002)130<2260:DHVIFG>2.0.CO;2.

Kraus, E. B., 1963: The diurnal precipitation change over the sea. *J. Atmos. Sci.,* **20,** 551–556, doi:10.1175/1520-0469(1963)020<0551:TDPCOT>2.0.CO;2.

Lajoie, F. A., and I. J. Butterworth, 1984: Oscillation of high-level cirrus and heavy precipitation around Australian region tropical cyclones. *Mon. Wea. Rev.,* **112,** 535–544, doi:10.1175/1520-0493(1984)112<0535:OOHLCA>2.0.CO;2.

Liu, C., and E. Zipser, 2014: Differences between the surface precipitation estimates from the TRMM precipitation radar and passive microwave radiometer version 7 products. *J. Hydrometeor.,* **15,** 2157–2175, doi:10.1175/JHM-D-14-0051.1.

Lonfat, M., F. D. Marks, and S. S. Chen, 2004: Precipitation distribution in tropical cyclones using the Tropical Rainfall Measuring Mission (TRMM) Microwave Imager: A global perspective. *Mon. Wea. Rev.,* **132,** 1645–1660, doi:10.1175/1520-0493(2004)132<1645:PDITCU>2.0.CO;2.

Molinari, J., and S. Skubis, 1985: Evolution of the surface wind field in an intensifying tropical cyclone. *J. Atmos. Sci.,* **42,** 2865–2879, doi:10.1175/1520-0469(1985)042<2865:EOTSWF>2.0.CO;2.

Nesbitt, S. W., and E. J. Zipser, 2003: The diurnal cycle of rainfall and convective intensity according to three years of TRMM measurements. *J. Climate,* **16,** 1456–1475, doi:10.1175/1520-0442-16.10.1456.

NGDC, 2004: 5-Minute Gridded Global Relief Data Collection (ETOPO5). NOAA/National Centers for Environmental Information, accessed 25 December 2005. [Available online at http://www.ngdc.noaa.gov/mgg/fliers/93mgg01.html.]

NOAA/National Climatic Data Center, 2014: IBTrACS-All data, version v03r06. NOAA/National Climatic Data Center. Subset used: 1998–2012, accessed 23 September 2013. [Available online at http://www.ncdc.noaa.gov/ibtracs/index.php?name=ibtracs-data.]

Randall, D. A., Harshvardhan, and D. A. Dazlich, 1991: Diurnal variability of the hydrologic cycle in a general circulation model. *J. Atmos. Sci.,* **48,** 40–63, doi:10.1175/1520-0469(1991)048<0040:DVOTHC>2.0.CO;2.

Rodgers, E. B., and R. F. Adler, 1981: Tropical cyclone rainfall characteristics as determined from a satellite passive microwave radiometer. *Mon. Wea. Rev.,* **109,** 506–521, doi:10.1175/1520-0493(1981)109<0506:TCRCAD>2.0.CO;2.

——, and H. F. Pierce, 1995: A satellite observational study of precipitation characteristics in western North Pacific tropical cyclones. *J. Appl. Meteor.,* **34,** 2587–2599, doi:10.1175/1520-0450(1995)034<2587:ASOSOP>2.0.CO;2.

Romatschke, U., S. Medina, and R. A. Houze, 2010: Regional, seasonal, and diurnal variations of extreme convection in the South Asian region. *J. Climate,* **23,** 419–439, doi:10.1175/2009JCLI3140.1.

Serra, Y. L., and M. J. McPhaden, 2004: In situ observations of diurnal variability in rainfall over the tropical Pacific and Atlantic Oceans. *J. Climate,* **17,** 3496–3509, doi:10.1175/1520-0442(2004)017<3496:ISOODV>2.0.CO;2.

Tuleya, R. E., 1994: Tropical storm development and decay: Sensitivity to surface boundary conditions. *Mon. Wea. Rev.,* **122,** 291–304, doi:10.1175/1520-0493(1994)122<0291:TSDADS>2.0.CO;2.

Wu, Q., Z. Ruan, D. Chen, and T. Lian, 2015: Diurnal variations of tropical cyclone precipitation in the inner and outer rainbands. *J. Geophys. Res.,* **120,** 1–11, doi:10.1002/2014JD022190.

Zagrodnik, J. P., and H. Jiang, 2013: Comparison of TRMM precipitation radar and microwave imager rainfall retrievals in tropical cyclone inner cores and rainbands. *J. Geophys. Res.,* **118,** 29–42, doi:10.1029/2012JD017919.